1 **Blockade of SARS-CoV-2 infection in vitro by highly potent PI3K-**

2 **α/mTOR/BRD4 inhibitor**

3 **Authors:** Arpan Acharya[1], Kabita Pandey[1], Michellie Thurman[1], Kishore B. Challagundala[2],

4 Kendra R. Vann[3], Tatiana G. Kutateladze[3], Guillermo A Morales[4], Donald L. Durden*[4,5,6],

5 Siddappa N. Byrareddy*[1,2,7].

6 **Affiliations:**

7 [1]Department of Pharmacology and Experimental Neuroscience, University of Nebraska Medical

8 Center; Omaha, NE 68131, USA.

9 [2]Department of Biochemistry and Molecular Biology, University of Nebraska Medical Centre,

10 Omaha, NE, 68131, USA

11 [3]Department of Pharmacology, University of Colorado School of Medicine; Aurora, CO 80045,

12 USA.

13 [4]SignalRx Pharmaceuticals, Inc.; Cumming, GA 30041, USA.

14 [5]Division of Pediatric Hematology-Oncology, Department of Pediatrics, Moores Cancer Center,

15 UC San Diego School of Medicine; La Jolla, CA 92130, USA.

16 [6]Levine Cancer Institute; Charlotte, NC 28204, USA.

17 [7] Department of Genetics, Cell Biology, and Anatomy, University of Nebraska Medical Centre,

18 Omaha, NE, 68131, USA.

19 *Corresponding authors.

20

21 Email: sid.byrareddy@unmc.edu; ddurden@uscd.edu

22

23 **One Sentence Summary:** Evidence of *in silico* designed chemotype (SF2523) targeting PI3K-

24 α/mTOR/BRD4 inhibits SARS-CoV-2 infection and is highly synergistic with remdesivir.

25

26   **Abstract:**

27   Pathogenic viruses like SARS-CoV-2 and HIV hijack the host molecular machinery to establish

28   infection and survival in infected cells. This has led the scientific community to explore the

29   molecular mechanisms by which SARS-CoV-2 infects host cells, establishes productive

30   infection, and causes life-threatening pathophysiology. Very few targeted therapeutics for

31   COVID-19 currently exist, such as remdesivir. Recently, a proteomic approach explored the

32   interactions of 26 of 29 SARS-CoV-2 proteins with cellular targets in human cells and identified

33   67 interactions as potential targets for drug development. Two of the critical targets, the

34   bromodomain and extra-terminal domain proteins (BETs): BRD2/BRD4 and mTOR, are

35   inhibited by the dual inhibitory small molecule SF2523 at nanomolar potency. SF2523 is the

36   only known mTOR PI3K-α/(BRD2/BRD4) inhibitor with potential to block two orthogonal

37   pathways necessary for SARS-CoV-2 pathogenesis in human cells. Our results demonstrate that

38   SF2523 effectively blocks SARS-CoV-2 replication in lung bronchial epithelial cells *in vitro*,

39   showing an IC_{50} value of 1.5 µM, comparable to IC_{50} value of remdesivir (1.1 µM). Further, we

40   demonstrated that the combination of doses of SF2523 and remdesivir is highly synergistic: it

41   allows for the reduction of doses of SF2523 and remdesivir by 25-fold and 4-fold, respectively,

42   to achieve the same potency observed for a single inhibitor. Because SF2523 inhibits two SARS-

43   CoV-2 driven pathogenesis mechanisms involving BRD2/BRD4 and mTOR signaling, our data

44   suggest that SF2523 alone or in combination with remdesivir could be a novel and efficient

45   therapeutic strategy to block SARS-CoV-2 infection and hence be beneficial in preventing severe

46   COVID-19 disease evolution.

47

48

49 **INTRODUCTION**

50   Coronavirus disease 2019 (COVID-19) is caused by a novel coronavirus named severe

51 acute respiratory syndrome coronavirus 2 (SARS-CoV-2) (*1*). This is a novel zoonotic single-

52 stranded RNA virus that belongs to the betacoronavirus family, which also includes severe acute

53 respiratory syndrome coronavirus (SARS-CoV) and middle east respiratory syndrome

54 coronavirus (MERS-CoV) (*2*). The ongoing global pandemic of SARS-CoV-2 was first reported

55 from Wuhan, China, in January 2020. As of March 01, 2021, globally, more than 114.30 million

56 confirmed cases and 2.53 million deaths had been reported due to COVID-19

57 (https://coronavirus.jhu.edu/map.html).

58 SARS-CoV-2 utilizes host cell angiotensin-converting enzyme 2 (ACE2) as the primary receptor

59 for entry along with several other accessory factors that include TMPRSS2, neuropilin-1,

60 PIKFyve kinase, and CD147, among others (*3-8*). After internalization, cathepsin L cleaves the S

61 protein and aids in releasing the viral genome in the host cell cytoplasm (*3*). Inside the cell, virus

62 utilizes the host cell machinery to replicate its positive-sense RNA genome and process the

63 polyproteins to generate functional structural and nonstructural proteins. Then, the viral genome

64 and structural proteins are assembled into progeny viruses, travel to the plasma membrane and

65 are released utilizing lysosomal exocytosis pathways (*9*). During this replication cycle, several

66 viral proteins like NSP1, NSP3, and ORF7a/b suppress the type 1 interferon (IFN) mediated host

67 immune response (*10*), while others activate Toll-like receptors (TLRs) that stimulate the release

68 of proinflammatory cytokines like IL-1β, IL-2, IL-6, IL-7, GCSF, IFN-γ, and TNF-α (*11*).

69 The pathophysiology of COVID-19 follows a biphasic pattern. In contrast, the initial acute phase

70 of infection is manifested by viral infection-driven symptoms including sore throat, fever,

71 fatigue, dry cough, and/or diarrhea (*12*). In severely ill patients, this is followed by an

72   immunopathologic phase that includes the development of acute respiratory distress syndrome

73   (ARDS), systemic inflammation, and cytokine storm, which is responsible for multiple organ

74   failure and a higher rate of fatalities (*1*). Patients with certain comorbid conditions like

75   hypertension, cardiovascular disease, diabetes, and chronic obstructive pulmonary disorders

76   (COPD) also have a higher probability of developing acute severe respiratory distress syndrome

77   (ARDS). Moreover, a subpopulation of patient's develops neurological disease manifestations

78   like loss of taste and smell, dizziness, confusion, ataxia, seizures and Guillain-Barré Syndrome

79   (GBS) have also been reported (*13*). Among the patients who develop ARDS, many of them

80   succumbed to the disease due to the development of pulmonary fibrosis (*14*). These data suggest

81   that the addition of a currently available or upcoming anti-fibrotic agent for the management of

82   critically ill COVID-19 patients would be beneficial to reduce the rate of fatalities and long-term

83   consequences of pulmonary fibrosis.

84   Although some vaccine candidates received emergency use authorization (EUA) from U.S. Food

85   and Drug Administration (USFDA) to control the rapid spread of the virus, it is anticipated that it

86   will take several months to years to vaccinate the majority of the population (*15*). Again the

87   long-term safety, efficacy, and durability of these vaccines remain unknown specifically for the

88   'special' populations that include children, pregnant women, individuals with comorbid

89   conditions that may impact immune response against a vaccine (*16*). Along with that,

90   preliminary studies indicate that the emerging new strains of SARS-CoV-2 from South Africa

91   having Lys417Asn, Glu484Lys, and Asn501Tyr substitutions in the receptor-binding domain,

92   and Leu18Phe, Asp80Ala, Asp215Gly, 242–244del, and Arg246Ile in the N-terminal domain of

93   spike protein have reduced susceptibility to neutralization by convalescent plasma therapy (*17*).

94   These results question the efficacy of the spike protein-based vaccines against new strains of the

95   virus and further support the fact that this virus will eventually enter an endemic stage with

96   world-wide distribution and high-level mortality. Therefore, other strategies to reduce SARS-

97   CoV-2 and related mutant strain associated morbidity and mortality are urgently needed.

98   These factors underscore the urgent development of an effective therapeutic regimen that will

99   control the rapid spread of the virus and reduce the high rate of fatalities among severely ill

100   patients. From the outset of this pandemic, multiple therapeutic strategies have been tested that

101   are at different stages of development and clinical trials with mixed responses (*18*). The majority

102   of which includes SARS-CoV-2 fusion/entry inhibitors (*19*), RNA-dependent RNA polymerases

103   (RdRps) inhibitors (*20*), viral protease inhibitors (*21*), several classes of immune-suppressive

104   agents to control systemic hyperactive inflammatory response (*22*), and cytokine storm and

105   convalescent plasma treatment (*23*).

106   At present, remdesivir (GS-5734) is the only US FDA-approved antiviral agent in use to treat

107   COVID-19 (*24*). It is a prodrug of a monophosphate nucleotide analog that selectively inhibits

108   RNA-dependent RNA polymerase of SARS-CoV-2 (*25*). A randomized, double-blind, placebo-

109   controlled clinical trial reported shorter hospital stay for patients with COVID-19 when treated

110   with remdesivir than placebo controls (ClinicalTrials.gov: NCT04280705) (*26*). However,

111   another multicenter, randomized clinical trial conducted by WHO did not find any superior effect

112   of remdesivir on hospitalized COVID-19 patients (ClinicalTrials.gov: NCT04315948) (*27*).

113   Therefore, in the absence of a fully effective drug in the prevention of COVID-19, it is warranted

114   to identify and validate more compounds that, individually or in combination with other

115   molecules, will have a profound antiviral efficacy against COVID-19 (*28*).

116   Recently, Gordon et al. (*29*) used a proteomic approach to explore the interactions of 26 out of

117   29 SARS-CoV-2 proteins with cellular targets in human cells and identified 67 potential

118   interactions and targets for drug development. By molecular pathway analysis, they

119   demonstrated an interaction of BRD2/BRD4 with E protein of SARS-CoV-2. In another study

120   Tian et al. using CRISPRi screening shown that BRD2 inhibition down regulate the ACE2

121   expression which block the entry of SARS-CoV-2 within host cells as well as control

122   hyperactive immune response in COVID-19 patients through down regulations of ISGs (*30*).

123   Therefore, they proposed BRD2 as a potential target for development of therapeutics against

124   SARS-CoV-2. Two of the critical host factors responsible for pathogenesis of SARS-CoV-2, the

125   bromodomain and extra-terminal domain proteins (BETs): BRD2/BRD4 and mTOR, are

126   inhibited by the dual inhibitory small molecule SF2523 developed by our group previously. In

127   the present study our *in vitro* data using a human bronchial epithelial cell line (UNCN1T) shows

128   that SF2523 effectively blocks SARS-CoV-2 replication with IC_{50} values comparable to that of

129   remdesivir. We also found that the combination of doses of SF2523 and remdesivir is highly

130   synergistic. There is a 25-fold dose reduction for SF2523 and a 4-fold dose reduction for

131   remdesivir, respectively, when the two compounds are used in combination and they maintain

132   similar potency as a single compound. Future studies in suitable animal models are needed to

133   establish the clinical efficacy of SF2523 alone or a fixed-dose combination of SF2523 and

134   remdesivir as a novel treatment of COVID-19.

135

136   **RESULTS**

137   **Molecular interaction of SF2523 with PI3K-α and BRD4**

138   In a recent study using proteomic analysis, Gordon et al. (*29*) identified 67 host factors that

139   interact with SARS-CoV-2 proteins and represent potential drug development targets. Two of the

140   potential host targets identified, BETs BRD2/BRD4 and mTOR, are inhibited by SF2523.

141   Molecular modeling and structural analysis of predicted molecular interactions of dual BET

142   (BRD2/4)/PI3K-mTOR inhibitor SF2523 with the catalytic domain of PI3K-α are displayed in

143   the top panel of **Fig. 1.** The molecular interactions of SF2523 binding to BRD4-BD1 binding

144   pocket were observed from a 1.8 angstrom resolution crystal structure (PDB ID: 5U28) displayed

145   in the bottom panel of **Fig. 1**. In a cell-free system, the binding potential of SF2523 with its

146   potential targets is shown below the bottom panel of **Fig 1.**

147   **Antiviral efficacy of SF2523 and remdesivir**

148   This study evaluates SF2523 and remdesivir (GS-5734) antiviral efficacy against SARS-CoV-2

149   in Vero-STAT1 knockout cells and UNCN1T cells. STAT1 is a transcription factor essential for

150   interferon-mediated host-cell antiviral response. The STAT1 knockout cells are highly

151   susceptible to viral infection due to the absence of cellular antiviral response and used as control

152   for robust viral infection in this study. On the other hand, UNCN1T is a human bronchial

153   epithelial cell line and expected to demonstrate the *in vivo* pathogenesis of SARS-CoV-2 in the

154   lung and serves as a good *in vitro* model for testing efficacy of antiviral compounds against

155   SARS-CoV-2.

156   Both cell types were treated with SF2523 or remdesivir and their IC_{50} values were determined 24

157   hrs, and 48 hrs post-infection. The replication kinetics were determined from the culture

158   supernatant of SARS-CoV-2 infected UNCN1T and Vero-STAT1 knockout cells in the presence

159   of increasing concentrations of SF2523 and remdesivir and are described in **Fig. 2A** and **Fig. 2B**,

160   respectively. Both compounds show a substantial reduction in SARS-CoV-2 viral load 24 hrs

161   post-infection. Based on SARS-CoV-2 viral loads 24 hrs post infection, SF2523 showed

162   potential antiviral activity and inhibited infection in UNCN1T cells with an IC_{50} of 1.52 μM and

163   remdesivir with an IC_{50} of 1.06 μM. In Vero-STAT1 knockout cells, SF2523 has an IC_{50} of 1.02

164   μM and remdesivir has an IC_{50} of 1.03 μM (**Fig. 2C and 2D**). SARS-CoV-2 replication kinetics

165   48 hrs post-infection in SF2523 and remdesivir treated UNCN1T and Vero-STAT1 knockout

166   cells are described in **Fig. S1A** and **Fig. S1B,** respectively. SF2523 and remdesivir have an IC_{50}

167   value of 1.58 μM and 2.75 μM in UNCN1T cells (**Fig. S1C**) and IC_{50} of 3.22 μM and 0.76 μM

168   in Vero-STAT1 knockout cells (**Fig. S1D**), respectively.

169   **Dose-response relationship and synergy of SF2523 with remdesivir**

170   After testing SF2523 and remdesivir separately, we evaluated a series of combinations of doses

171   of SF2523 and remdesivir with concentrations above and below the IC_{50} determined above. In

172   UNCN1T cells at 24 hrs post-infection, we observed the best inhibitory dose combination. An

173   IC_{50} value of 0.62 μM was observed for remdesivir when combined with 0.1 μM SF2523 (**Fig.**

174   **3A**). Vice versa, we saw the inhibition of viral replication at a fixed remdesivir dose of 0.05 μM

175   and an IC_{50} value of 1.21 μM for SF2523. (**Fig. 3B**). The use of multiple drugs with a different

176   modes of action and synergistic effects is a standard for treatment of infectious diseases to

177   increase the overall efficacy of the therapy and reduce dosage of individual drugs while also

178   reducing the toxicity level and the chances of development of drug resistance (*31*).

179   Based on mass action law and the classic model of enzyme-substrate inhibitor interactions, the

180   median-effect equation was proposed by Chou (*32*), which describes the dose-effect relationship

181   as $(Fa/Fu) = (D/Dm)^m$ or $\log(Fa/Fu) = m\log(D) - m\log(Dm)$. Where the slope (m) of the lines

182   signifies the shape (m = 1, >1, and <1 signify hyperbolic, sigmoidal, and flat sigmoidal dose-

183   effect curves, respectively). Fa is defined as percentage inhibition of viral growth at dose D, and

184   Fu is the fraction that remains unaffected (i.e., Fu = 1 - Fa). The antilog of x-intercept, where

185   Fa/Fu = 1 or $\log(Fa/Fu) = 0$, gives the Dm value. [log(Dm)] signifies the potency of the drugs

186   (where Dm stands for median effective dose or IC_{50} concentration: The concentration required to

187   inhibit 50% growth of the virus). By extrapolating the median-effect equation for multiple drugs,

188   Chou and Talalay proposed the combination index (CI) theorem to quantify synergism and

189   antagonism between drug combinations (*33*). Low CI values with increased Fa values indicate

190   superior compatibility and high synergism between drugs combination (based on Chou and

191   Talalay Combination Index Theorem, CI < 1, = 1, and >1 show synergism, additive effect, and

192   antagonism, respectively). A plot of CI values at different fraction affected (Fa) levels referred to

193   as Fa-CI plot or the Chou-Talalay plot.

194   Using CompuSyn, we generated the Median-Effect plot (Chou plot) of remdesivir (red line),

195   SF2523 (blue line), and the fixed-dose combination of remdesivir and SF2523 (green line) for

196   SARS-CoV-2 infected UNCN1T cells 24 hrs post infection as described above (**Fig. 4A**).

197   Analysis of the Median-Effect, where the X-intercept of the lines indicates potency, shows that

198   the combination dose is more potent than the individual doses of the compounds. In contrast, the

199   Chou-Talalay plot (**Fig. 4B**) indicates the synergistic effect of SF2523 and remdesivir. The dose-

200   response percent inhibition matrix of single and combined treatment of remdesivir and SF2523

201   was computed using SynergyFinder v.2 (**Fig. 4C**). The 3-D interaction landscape between

202   remdesivir and SF2523 was calculated based on Loewe additive model using SynergyFinder v.2

203   in SARS-CoV-2 infected UNCN1T cells 24 hrs post-infection (Loewe synergy score 34.88; with

204   most synergistic area score of 40.24) (**Fig 4D**). Synergy maps highlight synergistic and

205   antagonistic dose regions in red and green colors, respectively. Although there is no defined

206   threshold, drug combinations with a synergy scores above -10 is considered likely antagonistic,

207   and a score between -10 to 10 is deemed a possible additive. Any score above 10 is considered

208   synergistic.

209   Similarly, for SARS-CoV-2 infected Vero-STAT1 knockout cells treated with different

210   combination doses of remdesivir and SF2523, the Median-Effect plot (Chou plot) of remdesivir

211   (red line), SF2523 (blue line), and the fixed-dose combination of remdesivir and SF2523 (green

212   line) is described in **Fig. 5A**, the Chou-Talalay plot (**Fig. 5B**) indicates a synergistic effect of

213   SF2523 and remdesivir. The dose-response percent inhibition matrix of single and combined

214   treatment of remdesivir and SF2523 was computed using SynergyFinder v.2 (**Fig. 5C**) and the 3-

215   D interaction landscape between remdesivir and SF2523 was calculated based on a Loewe

216   additive model using SynergyFinder v.2 in SARS-CoV-2 infected UNCN1T cells 24 hrs post-

217   infection (Loewe synergy score -0.20; with most synergistic area score of 7.67) (**Fig. 5D**).

218   **Table 1** indicates the median effective dose of SF2523, remdesivir, and their fixed-dose

219   combinations. Whereas **Table 2** shows the CI values at ED_{50}, ED_{75}, ED_{90}, and ED_{95} in VERO-

220   STAT1 knockout and UNCN1T cells, which suggests a moderate to strong synergistic effect of

221   the drug combinations. In Vero-STAT1 KO cells at Fa 0.5, we obtained a dose reduction index

222   (DRI) of 11.56 for SF2523 and 2.35 for remdesivir, respectively (with Fa for combination 0.452;

223   2.617 for SF2523 and 0.533 for remdesivir). On the other hand, in UNCN1T cells, we obtained a

224   dose reduction index (DRI) of 25.33 for SF2523 and 3.75 for remdesivir, respectively, (with Fa

225   for combination 0.145; 1.836 for SF2523 and 0.272 for remdesivir).

226   **NMR studies involving SF2523 and BRD4**

227   We note that remdesivir does not alter the potency of SF2523 and does not interfere with the

228   binding of SF2523 to BRD4. To confirm this interaction, we performed NMR titration

229   experiments using ^{15}N-labeled BRD4 domains and showed that remdesivir is incapable of

230   binding to either BD1, BD2, or the ET domain of BRD4, as no significant chemical shift

231   perturbations were observed in $^{1}H,^{15}N$ heteronuclear single quantum coherence (HSQC) spectra

232 of these domains (**Fig. 6**). However, the subsequent addition of SF2523 to the NMR samples of

233 BD1 and BD2 led to large resonance changes, indicating robust binding, and no binding of

234 SF2523 was detected to the ET domain of BRD4.

235

236 **DISCUSSION**

237 Other than remdesivir, a viral RNA-dependent RNA polymerase inhibitor (*34*), there are no

238 confirmed efficacious molecularly targeted therapeutic agents for the treatment of COVID-19.

239 Targeted therapies that exploit host-virus interaction are likely to be least impacted by the

240 emergence of mutated strains of SARS-CoV-2 and produce more robust, durable treatment

241 options. Gordon *et al*. identified two potential targets for SARS-CoV-2 infectivity, including

242 BRD4 and mTOR kinase pathway (*29*). Using an *in vitro* we show that SF2523 is as potent and

243 effective as remdesivir in blocking the SARS-CoV-2 cytotoxicity and infectivity at

244 concentrations that are achievable and efficacious in animal models (*35*). SF2523 is highly

245 selective and the only known dual inhibitor of PI3K-α/mTOR and BRD4 and is currently slated

246 for clinical development. Hence, it is an excellent candidate for further development for systemic

247 and pulmonary delivery for treatment of COVID-19. Importantly, SF2523 and multiple analogs

248 are the product of extensive *in silico* molecular design to engineer chemotypes with dual or triple

249 inhibitory properties against well-chosen synthetic lethality targets like BRD4, PI3K, and mTOR

250 (*36-38*)

251 The ATP catalytic site of PI3K-α is driven by a critical hydrogen-bond interaction with the NH of

252 Val851. The successful interaction of SF2523 as a PI3K inhibitor was designed with this mode of

253 action where the oxygen atom of the morpholine group engages as a hydrogen-bond acceptor with

254 the required NH of Val851. For the docking against PI3K, we initially created a p110-PI3K-α

11

255 homology model using the crystal structure of human-derived PI3K-γ (PDB ID: 1E7V) where the

256 human PI3K-α protein sequence was superimposed to the PI3K-γ protein sequence. The resulting

257 3D model of PI3K-α was subsequently used for docking of SF2523 where amino acids within a

258 10 Å radius at the ATP binding site were selected. Successful docking of SF2523 was achieved

259 using FlexX, where the optimal bin36ding mode of SF2523 fulfills 2 pharmacophoric

260 requirements, namely, the spatial location of the carbonyl group of SF2523 and a hydrogen-bond

261 interaction between the morpholine group of SF2523 and Val851 (*39*).

262 BRD4 bromodomain 1 (BRD4-BD1) active site recognizes acetylated lysine residues in histones

263 via hydrogen-bond interaction with the NH of the conserved Asn140 residue. This binding site is

264 a hydrophobic cavity that contains structurally conserved water molecules. For the docking of

265 SF2523 against BDR4-BD1, a human-derived BDR4-BD1 crystal structure co-crystallized with

266 small-molecule BRD4 inhibitor JQ1 (PDB ID: 3MXF) was obtained and amino acids within a 6

267 Å radius of JQ1 were selected. Using AutoDock Vina (*40*) and rDock (*41*), SF2523 was predicted

268 to bind, forming a hydrogen-bond interaction between the carbonyl group of SF2523 and the NH

269 of Asn140 and a conserved water molecule. The morpholine group of SF2523 is oriented towards

270 the opening of the binding site (solvent-exposed). The subsequent successful crystallization of

271 SF2523 with BRD4-BD1 (PDB ID: 5U28) confirmed the predicted binding interaction of SF2523

272 and it also revealed that one of the oxygen atoms of the benzodioxane moiety of SF2523 engages

273 in 2 additional hydrogen-bond interactions with BRD4-BD1, one with GLN85 and one with

274 another conserved water molecule (*35*). NMR data from our laboratory confirms interaction

275 between BRD4 BD1 and acetylated lysine with the C terminus of SARS-CoV-2 E protein. Also,

276 as per Zhang et al., other viral proteins have been shown to have functional interaction with BET

277 BRD4 for viral pathogenesis (*42*).

278   From previous experience, it was observed that in patients infected with SARS and MERS, the

279   viral load peaks only after a week of initial reporting of disease symptoms (*43, 44*). Whereas in

280   the case of SARS-CoV-2, similar to influenza, the viral load peaks along with the onset of

281   disease symptoms (*45*). It was reported that for influenza patients with high viral load at the

282   beginning of disease symptoms, combinational antiviral therapy is more effective than

283   monotherapies (*46, 47*). This is mirrored during the initial phase of the COVID-19 pandemic,

284   where multiple combinational therapeutic approaches using several repurposed drugs show mild

285   to moderate efficacy in treating severely ill patients (*48-50*). To extend this combinational

286   therapeutic approach to treat COVID-19 patients *in vitro,* we tested combination treatment of

287   SF2523 and remdesivir as described above. Our findings suggest that this drug combination is

288   highly synergistic in the human bronchial epithelial cell line with 25-fold dose reduction for

289   SF2523 and 4-fold dose reduction for remdesivir while maintaining similar therapeutic efficacy

290   of individual monotherapies. This reduction in remdesivir dose is also expected to reduce the

291   high incidence of adverse effects related to remdesivir monotherapy (*26, 51*).

292   To characterize the molecular basis for SF2523 mediated inhibition of SARS-CoV-2 replication

293   and confirm the synergistic combination of this compound with remdesivir *in vitro*, we used

294   NMR to look at the capacity of these two chemotypes to interact with BRD4-BD1, BRD4-BD2,

295   and BRD4-ET domains. Consistent with the substantial synergy noted with the two agents,

296   remdesivir did not bind to BRD4; however, SF2523 binds to both BD1 and BD2 but not the

297   extra-terminal (ET) domain of BRD4, supporting differential molecular pathways targeted by

298   these chemically distinct chemotypes. BRD2/BRD4 are epigenetic factors whose two N-

299   terminal bromodomains (BDs) bind with acetylated histones and regulate several proteins (*52*).

300   Several observations related to Gordon et al. (*29*) reporting that BRD4 binds to the SARS-CoV-2

301   E protein include: 1) the E protein forms a homopentameric cation-selective channel which is

302   required for viral budding and release from cells, 2) the E protein is a 72-residue viroporin

303   molecule, 3) mutations or deletions within the transmembrane channel attenuate viral

304   pathogenicity (*53*). Data from emerging mutant strains of SARS-CoV-2 strains indicates

305   presence of several variation in the C terminal domain E protein, that may impact its binding

306   with host protein PALS1with altered disease pathogenesis (*54*). BRD2/BRD4 also has a

307   significant role in cell cycle regulation, inflammation, and inhibition of BRD4 by SF2523

308   enhances the innate and adaptive immune response (*37*). Again, BRD4 drives the secretion of IL-

309   6, CXCL8, and IL17A, which leads to the development of idiopathic pulmonary fibrosis and

310   chronic obstructive pulmonary disease (COPD) (*55*). This suggests that BET inhibitors may

311   disrupt the interaction between BRDs and E protein and will have a favorable outcome in

312   treating COVID-19 patients. LARP1, a significant effector of the mTOR pathway, interacts with

313   nucleocapsid protein (N) (*56*). LARP1 knockdown of inhibitors of mTOR inhibits MERS

314   replication and have an immunosuppressive function (*57*). These data suggest potential important

315   interactions between the SARS-CoV-2 virion and the host machinery elements essential for viral

316   pathogenesis. Campbell et al., reported that SF2523 locks HIV replication in human cells via

317   induction of autophagy (*58*). Moreover, Joshi et al. reported that SF2523 has a potential

318   immunostimulatory impact on innate and adaptive T-cell immunity (*37*). Because SF2523

319   effectively targets two crucial elements of SARS-CoV-2 driven pathogenesis, BETs

320   BRD2/BRD4, and mTOR, and because of its immune activation activity, SF2523 can be a

321   potential therapeutic agent to control COVID-19. It can provide significant clinical benefit in

322   preventing profound COVID-19 disease evolution.

323   Our initial efforts to screen the efficacy of SF2523 monotherapy and combinational therapy

324   against SARS-CoV-2 in the 2D-cellular model is an essential step for initial screening of drug

325   like compounds before initiation of pre-clinical studies and commonly used to explore the

326   molecular mechanism of action. Our future studies will reveal their efficacy in pre-clinical

327   animal models of COVID-19. Its synergistic effect will result in a favorable shift in the plasma

328   Cmax/EC$_{90}$ ratio. Ongoing structural studies to elucidate the interaction of SF2523 with host

329   factors and viral targets will clarify mechanisms of efficacy, and potential resistance as the virus

330   continues to undergo mutagenesis and selection during the pandemic. Considering the emerging

331   data on the life cycle and biology of SARS-CoV-2 infection in humans and the rapid emergence

332   of mutant variants resistant to vaccine candidates, we suggest that a combinatorial approach

333   based on one small molecule which inhibits the interaction of multiple viral targets with host

334   factors necessary for viral pathogenesis will be required to control the mortality and morbidity

335   associated with the pandemic and the likely endemic phase of this disease globally.

336

337   In conclusion, our study demonstrates the *in vitro* efficacy of SF2523 as a monotherapy and in

338   combination with remdesivir against SARS-CoV-2 infection. Considering the marked

339   synergistic effect of these two molecules in a wide dose range in *in vitro* assays, we conclude

340   that, SF2523 alone or in combination with remdesivir represents a future therapeutic approach to

341   obviate the severe disease associated with the ongoing pandemic of SARS-CoV-2.

342

343

344

345

MATERIALS AND METHODS

Study design

In this *in vitro* study using a human bronchial epithelial cell line (UNCN1T) and Vero-STAT1

knockout cells, we evaluate the efficacy of SF2523 (PI3K-mTOR/BRD4 inhibitor) as a

monotherapy or in combination with remdesivir against SARS-CoV-2. Using NMR, we also

screen the interaction between different domains of BRD4 (BD1, BD2, and ET) and

SF2523/remdesivir.

Reagents, cell lines

Remdesivir (GS-5734) was obtained from Selleck Chemicals LLC, 14408 W Sylvanfield Drive,

Houston, TX 77014 USA. Vero E6 (ATCC® CRL-1586™) and Vero-STAT1 knockout cells

(ATCC® CCL-81-VHG™) were cultured in DMEM containing 10% fetal bovine serum, 2 mM

L-glutamine, penicillin (100 units/ml), streptomycin (100 units/mL), and 10 mM HEPES.

UNCN1T cells (a human bronchial epithelial cell line; Kerafast; cat# ENC011) were cultured

using BEGM media (Bronchial Epithelial Cell Growth Medium; Lonza: cat# CC-3170) in FNC

(Athena Enzyme Systems; cat# 0407) coated plates. All other molecular biology grade fine

chemicals used in the study were purchased from Sigma-Aldrich, St. Louis, MO, USA, unless

otherwise mentioned.

In silico docking of SF2523 against PI3K-α and BRD4-BD1.

The docking of SF-2523 with PI3K-α is described previously (*39*). *In silico* docking of SF2523

against BRD4-BD1 was performed using AutoDock Vina (*40*) and rDock (*41*). Crystal structure

of BRD4 (PDB ID 3MXF) was downloaded from the Protein Data Bank (*59*), residues and water

molecules within 6 Å^3 of JQ1 were kept, hydrogen atoms and charges were added, and SF2523

was docked using default parameters. A minimum of 150 docking solutions were recorded and the

16

369   conformation of SF2523 matching the expected binding mode (NH of Asn140 forming a hydrogen

370   bond with the carbonyl group of SF2523) with the strongest predicted binding energy was selected.

371   **Protein expression and purification**

372   The pGEX6P-BRD4 BD1 (amino acids 43-180) and pGEX4T-1 BRD4 BD2 (amino acids 342-

373   460) plasmids were expressed in Escherichia coli BL21 (DE3) RIL cells grown in M9 minimal

374   media supplemented with $^{15}NH_4Cl$ and purified as previously described (*35*). The bacteria cells

375   were harvested by centrifugation, resuspended in 10 mM HEPES pH 7.5, 150 mM NaCl, 1 mM

376   TCEP supplemented with DNase I and lysed by sonication. The BRD4 BD1 and BD2 constructs

377   were purified from the cleared lysate using glutathione Sepharose 4B beads and the GST tag was

378   cleaved with PreScission or thrombin protease. The protein was purified using a S100 column

379   (GE Healthcare) equilibrated in 10 mM HEPES pH 7.5, 150 mM NaCl, 1 mM TCEP. BD1

380   protein fractions were assessed for purity (95%) by SDS-PAGE, buffer exchanged into 1X PBS

381   (37 mM NaCl, 2.7 mM KCl, 4.3 mM Na2HPO4, 1.47 mM KH_2PO_4 supplemented with 5 mM

382   DTT and concentrated to ~10-20 mg/mL using 3 kDa Millipore concentrator and stored at -80

383   °C.

384   The pET32a-BRD4 ET domain (amino acids 600-700) vector was obtained from Timothy

385   McKinsey. The N-terminal TRX-6His-S-tagged ET domain was expressed in Escherichia coli

386   Tuner (DE3) competent cells using M9 minimal media supplemented with $^{15}NH_4Cl$. Cells were

387   induced with 0.5 mM IPTG, cultured for 16 h post-induction at 18 °C, and harvested at 5000

388   rpm. The His-tagged protein was purified with Nickel-NTA resin (Thermo Scientific) in 20 mM

389   Sodium Phosphate (pH 7.0) buffer, supplemented with 500 mM NaCl, 10 mM imidazole and 2

390   mM BME. The tagged protein was eluted using a 30-300 mM imidazole gradient elution. The

391   eluted protein was buffer exchanged into cleavage buffer containing 20 mM Tris pH 8.0, 50 mM

17

392   NaCl, 2 mM CaCl2 and the TRX-6His-S-tag was cleaved overnight at RT with enterokinase

393   protease (NEB). The ET domain was further purified using Nickel-NTA resin (Thermo

394   Scientific) to remove the cleaved tag. Size-exclusion chromatography was performed using a

395   Superdex S75 column. The purified protein was buffer exchanged into 20 mM Tris pH 7.0, 100

396   mM NaCl, 5 mM DTT and concentrated to ~10 mg/mL using 3 kDa Millipore concentrator and

397   stored at -80 °C.

398   **NMR Experiments**

399   For BRD4 BD1 or BD2 experiments, samples containing 0.2 mM ^{15}N-labeled BRD4 BD1/BD2

400   in 1X PBS, 5 mM DTT, and 10% D_2O were prepared. For BRD4 ET experiments, samples

401   containing 0.15 mM ^{15}N-labeled BRD4 ET domain in 20 mM Tris pH 7.0, 100 mM NaCl, 5 mM

402   DTT, and 10% D_2O were prepared. Remdesivir (Selleck Chemicals) and SF2523 (SignalRx

403   Pharmaceuticals, Inc.) were dissolved in 100% DMSO. Remdesivir was titrated into each NMR

404   sample up to 5 molar equivalents. Subsequently, SF2523 was added at a 1:2 equivalence. Two-

405   dimensional ^{1}H,^{15}N HSQC spectra were acquired on a 600 MHz Varian spectrometer fitted with

406   a cryogenic probe at 298 K. Spectra were processed with NMRPipe.

407   **Production of SARS-CoV-2 stocks**

408   SARS-CoV-2 isolate USA-WI1/2020 (BEI; cat# NR-52384) was procured from BEI and

409   passaged in Vero-STAT1 knockout cells. The viral titer was determined using plaque assay (*60*).

410   In brief, Vero E6 cells were seeded in 6-well plates. After 24 hrs, cells were washed with sterile

411   1X PBS. The viral stock was serially diluted and added to cells in duplicate with fresh media and

412   the plates were incubated at 37 ˚C for 1 hour with occasional shaking every 15 minutes. Then 2

413   mL of 0.5% agarose in minimal essential media (MEM) containing 5% FBS and antibiotics was

414   added per well. Plates were incubated at 37 ˚C for 72 hours. Then the cells were fixed with 4%

18

415 paraformaldehyde overnight, followed by the removal of the overlay and then stained with 0.2%

416 crystal violet to visualize plaque forming units (PFU). All assays involving live SARS-CoV-2

417 were performed in University of Nebraska Medical Center (UNMC) BSL-3 core laboratory

418 setting and approved by the University of Nebraska Medical Center institutional Biosafety

419 Committee (IBC) with the approval number 20-05-029-BL3.

420 **Measuring the antiviral potential of SF2523 and remdesivir against SARS-CoV-2:**

421 UNCN1T and Vero-STAT1 knockout cells were seeded in 96-well plates 24 hours before

422 infection at 20,000 cells/well. Different concentrations of SF2523 and remdesivir (100 μM, 10

423 μM, 5 μM, 1 μM, 0.1 μM, 0.01 μM and 0.001 μM) were added to the cells 2 hours before

424 infection. The cells were infected with 0.1 MOI of SARS-CoV-2 using Opti-MEM I reduced

425 serum medium (Thermo Fisher, Cat#31985062) and incubated for 1 hour at 37 °C with 5% CO_2.

426 For positive control, cells were treated with same volume of DMSO equivalent to the volume of

427 drugs added. Mock infected cells received only Opti-MEM I reduced serum medium. At the end

428 of incubation virus inoculum was removed, cells were washed with 1X PBS 3 times and fresh

429 media supplemented with same concentration of drugs was added. Culture supernatant was

430 collected at 24 hrs and 48 hrs post infection. The SARS-CoV-2 viral load was quantified in

431 culture supernatant using RT-QPCR with primer probes targeting E gene of SARS-CoV-2 using

432 PrimeDirect Probe RT-qPCR Mix (TaKaRa Bio USA, Inc) and Applied Biosystems

433 QuantStudio3 real-time PCR system (Applied Biosystems, Waltham, MA, USA) per the

434 manufacturer's instructions. Primers and probes used for SARS-CoV-2 RNA quantification were

435 as follows: E_Sarbeco_F1: 5' – ACAGGTACGTTAATAGTTAATAGCGT – 3' (400 nM),

436 E_Sarbeco_R2: 5' – ATATTGCAGCAGTACGCACACA – 3' (400 nM) and E_Sarbeco_P1: 5'

437 – FAM - ACACTAGCCATCCTTACTGCGCTTCG - BHQ1 – 3' (200 nM) as recommended by

19

438   WHO. The SARS-CoV-2 genome equivalent copies were calculated using quantitative PCR

439   (qPCR) control RNA from heat-inactivated SARS-CoV-2, isolate USA-WA1/2020 (BEI; cat#

440   NR-52347). The percentage inhibition of SARS-CoV-2 replication in SF2523 and remdesivir

441   treated wells were calculated with respect to viral concentration in positive control wells that

442   were treated with DMSO (considered 0% inhibition) and negative control wells (uninfected

443   cells). IC_{50} values were calculated using four parameter variable slope sigmoidal dose-response

444   models using Graph Pad Prism 8.0 software.

445   **Measuring the combinational antiviral potential of SF2523 and remdesivir**

446   To determine possible combinational antiviral effect of SF2523 and remdesivir against SARS-

447   CoV-2, we tested 5 (remdesivir) X 4 (SF2523) dose combinations in SARS-CoV-2 infected

448   UNCN1T and Vero-STAT1 knockout cells. The percentage inhibition of viral replication for

449   each dose combinations were determined by RT-QPCR as described above. In brief, the

450   UNCN1T and Vero-STAT1 knockout cells were seeded in 96-well plates at a density of 20,000

451   cells/wells 24 hrs before infection. Two hours before infection the cells were treated with

452   different combination doses of SF2523 and remdesivir, infected with 0.1 MOI of SARS-CoV-2.

453   Twenty-four hours post infection culture supernatant was collected and SARS-CoV-2 viral load

454   was quantified using RT-QPCR as described above. The percentage inhibition of SARS-CoV-2

455   replication in the culture supernatant by different combined doses of SF2523 and remdesivir

456   were determined with respect to viral concentration in positive control wells that were treated

457   with DMSO (considered 0% inhibition) and negative control wells (uninfected cells). Then the

458   percent inhibition of viral replication for 1:1 fixed dose combination of the drugs was used to

459   generate CI-Fa, isobologram and dose-response plots. The combination index (CI) was

460   calculated using multiple drug effect equation developed by Chou and Talalay using the

20

461 CompuSyn algorithm (https://www.combosyn.com). A CI values of <1 indicate synergy, values

462 >1 indicate antagonism, and values equal to 1 indicate additive effects (*31, 33, 61*). Dose-

463 response percent inhibition matrix of single and combined treatment of remdesivir and SF2523

464 in SARS-CoV-2 infected UNCN1T and Vero-STAT1 knockout cells 24 hrs post infection and 3-

465 D interaction landscape between remdesivir and SF2523 were calculated based on Loewe

466 additive model using SynergyFinder v.2 (*62*).

467 **Statistical analysis**

468 IC_{50} values were calculated using four parameter variable slope sigmoidal dose-response models

469 using Graph Pad Prism 8.0 software. The combination index (CI) was calculated using multiple

470 drug effect equation developed by Chou and Talalay using the CompuSyn algorithm

471 (https://www.combosyn.com). 3-D interaction landscape between remdesivir and SF2523 was

472 calculated based on Loewe additive model using SynergyFinder v.2.

473

474 **References:**

475 1. H. A. Rothan, S. N. Byrareddy, The epidemiology and pathogenesis of coronavirus disease

476 (COVID-19) outbreak. *J Autoimmun* **109**, 102433 (2020).

477 2. G. Guo, L. Ye, K. Pan, Y. Chen, D. Xing, K. Yan, Z. Chen, N. Ding, W. Li, H. Huang, L.

478 Zhang, X. Li, X. Xue, New Insights of Emerging SARS-CoV-2: Epidemiology, Etiology,

479 Clinical Features, Clinical Treatment, and Prevention. *Front Cell Dev Biol* **8**, 410 (2020).

480 3. R. K. Suryawanshi, R. Koganti, A. Agelidis, C. D. Patil, D. Shukla, Dysregulation of Cell

481 Signaling by SARS-CoV-2. *Trends Microbiol*, (2020).

482 4. X. Ou, Y. Liu, X. Lei, P. Li, D. Mi, L. Ren, L. Guo, R. Guo, T. Chen, J. Hu, Z. Xiang, Z.

483 Mu, X. Chen, J. Chen, K. Hu, Q. Jin, J. Wang, Z. Qian, Characterization of spike

484   glycoprotein of SARS-CoV-2 on virus entry and its immune cross-reactivity with SARS-

485   CoV. *Nat Commun* **11**, 1620 (2020).

486   5.   P. Xia, A. Dubrovska, Tumor markers as an entry for SARS-CoV-2 infection? *FEBS J* **287**,

487   3677-3680 (2020).

488   6.   L. Cantuti-Castelvetri, R. Ojha, L. D. Pedro, M. Djannatian, J. Franz, S. Kuivanen, F. van

489   der Meer, K. Kallio, T. Kaya, M. Anastasina, T. Smura, L. Levanov, L. Szirovicza, A.

490   Tobi, H. Kallio-Kokko, P. Osterlund, M. Joensuu, F. A. Meunier, S. J. Butcher, M. S.

491   Winkler, B. Mollenhauer, A. Helenius, O. Gokce, T. Teesalu, J. Hepojoki, O. Vapalahti,

492   C. Stadelmann, G. Balistreri, M. Simons, Neuropilin-1 facilitates SARS-CoV-2 cell entry

493   and infectivity. *Science* **370**, 856-860 (2020).

494   7.   J. L. Daly, B. Simonetti, K. Klein, K. E. Chen, M. K. Williamson, C. Anton-Plagaro, D. K.

495   Shoemark, L. Simon-Gracia, M. Bauer, R. Hollandi, U. F. Greber, P. Horvath, R. B.

496   Sessions, A. Helenius, J. A. Hiscox, T. Teesalu, D. A. Matthews, A. D. Davidson, B. M.

497   Collins, P. J. Cullen, Y. Yamauchi, Neuropilin-1 is a host factor for SARS-CoV-2

498   infection. *Science* **370**, 861-865 (2020).

499   8.   M. Hoffmann, H. Kleine-Weber, S. Schroeder, N. Kruger, T. Herrler, S. Erichsen, T. S.

500   Schiergens, G. Herrler, N. H. Wu, A. Nitsche, M. A. Muller, C. Drosten, S. Pohlmann,

501   SARS-CoV-2 Cell Entry Depends on ACE2 and TMPRSS2 and Is Blocked by a Clinically

502   Proven Protease Inhibitor. *Cell* **181**, 271-280 e278 (2020).

503   9.   S. Ghosh, T. A. Dellibovi-Ragheb, A. Kerviel, E. Pak, Q. Qiu, M. Fisher, P. M. Takvorian,

504   C. Bleck, V. W. Hsu, A. R. Fehr, S. Perlman, S. R. Achar, M. R. Straus, G. R. Whittaker,

505   C. A. M. de Haan, J. Kehrl, G. Altan-Bonnet, N. Altan-Bonnet, beta-Coronaviruses Use

506 Lysosomes for Egress Instead of the Biosynthetic Secretory Pathway. *Cell* **183**, 1520-1535

507 e1514 (2020).

508 10. H. Xia, Z. Cao, X. Xie, X. Zhang, J. Y. Chen, H. Wang, V. D. Menachery, R. Rajsbaum,

509 P. Y. Shi, Evasion of Type I Interferon by SARS-CoV-2. *Cell Rep* **33**, 108234 (2020).

510 11. P. Conti, G. Ronconi, A. Caraffa, C. E. Gallenga, R. Ross, I. Frydas, S. K. Kritas, Induction

511 of pro-inflammatory cytokines (IL-1 and IL-6) and lung inflammation by Coronavirus-19

512 (COVI-19 or SARS-CoV-2): anti-inflammatory strategies. *J Biol Regul Homeost Agents*

513 **34**, 327-331 (2020).

514 12. G. Pascarella, A. Strumia, C. Piliego, F. Bruno, R. Del Buono, F. Costa, S. Scarlata, F. E.

515 Agro, COVID-19 diagnosis and management: a comprehensive review. *J Intern Med* **288**,

516 192-206 (2020).

517 13. A. Acharya, B. D. Kevadiya, H. E. Gendelman, S. N. Byrareddy, SARS-CoV-2 Infection

518 Leads to Neurological Dysfunction. *J Neuroimmune Pharmacol* **15**, 167-173 (2020).

519 14. P. M. George, A. U. Wells, R. G. Jenkins, Pulmonary fibrosis and COVID-19: the potential

520 role for antifibrotic therapy. *Lancet Respir Med* **8**, 807-815 (2020).

521 15. B. M. Prubeta, Current State of the First COVID-19 Vaccines. *Vaccines (Basel)* **9**, (2021).

522 16. M. Connors, B. S. Graham, H. C. Lane, A. S. Fauci, SARS-CoV-2 Vaccines: Much

523 Accomplished, Much to Learn. *Ann Intern Med*, (2021).

524 17. H. Tegally, E. Wilkinson, R. J. Lessells, J. Giandhari, S. Pillay, N. Msomi, K. Mlisana, J.

525 N. Bhiman, A. von Gottberg, S. Walaza, V. Fonseca, M. Allam, A. Ismail, A. J. Glass, S.

526 Engelbrecht, G. Van Zyl, W. Preiser, C. Williamson, F. Petruccione, A. Sigal, I. Gazy, D.

527 Hardie, N. Y. Hsiao, D. Martin, D. York, D. Goedhals, E. J. San, M. Giovanetti, J.

528 Lourenco, L. C. J. Alcantara, T. de Oliveira, Sixteen novel lineages of SARS-CoV-2 in

529 South Africa. *Nat Med*, (2021).

530 18. H. Li, Y. Zhou, M. Zhang, H. Wang, Q. Zhao, J. Liu, Updated Approaches against SARS-

531 CoV-2. *Antimicrob Agents Chemother* **64**, (2020).

532 19. S. Xiu, A. Dick, H. Ju, S. Mirzaie, F. Abdi, S. Cocklin, P. Zhan, X. Liu, Inhibitors of SARS-

533 CoV-2 Entry: Current and Future Opportunities. *J Med Chem* **63**, 12256-12274 (2020).

534 20. R. Pokhrel, P. Chapagain, J. Siltberg-Liberles, Potential RNA-dependent RNA polymerase

535 inhibitors as prospective therapeutics against SARS-CoV-2. *J Med Microbiol* **69**, 864-873

536 (2020).

537 21. B. Luan, T. Huynh, X. Cheng, G. Lan, H. R. Wang, Targeting Proteases for Treating

538 COVID-19. *J Proteome Res* **19**, 4316-4326 (2020).

539 22. A. H. Mansourabadi, M. Sadeghalvad, H. R. Mohammadi-Motlagh, N. Rezaei, The

540 immune system as a target for therapy of SARS-CoV-2: A systematic review of the current

541 immunotherapies for COVID-19. *Life Sci* **258**, 118185 (2020).

542 23. S. T. H. Liu, H. M. Lin, I. Baine, A. Wajnberg, J. P. Gumprecht, F. Rahman, D. Rodriguez,

543 P. Tandon, A. Bassily-Marcus, J. Bander, C. Sanky, A. Dupper, A. Zheng, F. T. Nguyen,

544 F. Amanat, D. Stadlbauer, D. R. Altman, B. K. Chen, F. Krammer, D. R. Mendu, A. Firpo-

545 Betancourt, M. A. Levin, E. Bagiella, A. Casadevall, C. Cordon-Cardo, J. S. Jhang, S. A.

546 Arinsburg, D. L. Reich, J. A. Aberg, N. M. Bouvier, Convalescent plasma treatment of

547 severe COVID-19: a propensity score-matched control study. *Nat Med* **26**, 1708-1713

548 (2020).

549   24.   H. X. J. Lin, S. Cho, V. Meyyur Aravamudan, H. Y. Sanda, R. Palraj, J. S. Molton, I.

550   Venkatachalam, Remdesivir in Coronavirus Disease 2019 (COVID-19) treatment: a review

551   of evidence. *Infection*, (2021).

552   25.   J. A. Al-Tawfiq, A. H. Al-Homoud, Z. A. Memish, Remdesivir as a possible therapeutic

553   option for the COVID-19. *Travel Med Infect Dis* **34**, 101615 (2020).

554   26.   J. H. Beigel, K. M. Tomashek, L. E. Dodd, A. K. Mehta, B. S. Zingman, A. C. Kalil, E.

555   Hohmann, H. Y. Chu, A. Luetkemeyer, S. Kline, D. Lopez de Castilla, R. W. Finberg, K.

556   Dierberg, V. Tapson, L. Hsieh, T. F. Patterson, R. Paredes, D. A. Sweeney, W. R. Short,

557   G. Touloumi, D. C. Lye, N. Ohmagari, M. D. Oh, G. M. Ruiz-Palacios, T. Benfield, G.

558   Fatkenheuer, M. G. Kortepeter, R. L. Atmar, C. B. Creech, J. Lundgren, A. G. Babiker, S.

559   Pett, J. D. Neaton, T. H. Burgess, T. Bonnett, M. Green, M. Makowski, A. Osinusi, S.

560   Nayak, H. C. Lane, A.-S. G. Members, Remdesivir for the Treatment of Covid-19 - Final

561   Report. *N Engl J Med* **383**, 1813-1826 (2020).

562   27.   W. H. O. S. T. Consortium, H. Pan, R. Peto, A. M. Henao-Restrepo, M. P. Preziosi, V.

563   Sathiyamoorthy, Q. Abdool Karim, M. M. Alejandria, C. Hernandez Garcia, M. P. Kieny,

564   R. Malekzadeh, S. Murthy, K. S. Reddy, M. Roses Periago, P. Abi Hanna, F. Ader, A. M.

565   Al-Bader, A. Alhasawi, E. Allum, A. Alotaibi, C. A. Alvarez-Moreno, S. Appadoo, A.

566   Asiri, P. Aukrust, A. Barratt-Due, S. Bellani, M. Branca, H. B. C. Cappel-Porter, N.

567   Cerrato, T. S. Chow, N. Como, J. Eustace, P. J. Garcia, S. Godbole, E. Gotuzzo, L.

568   Griskevicius, R. Hamra, M. Hassan, M. Hassany, D. Hutton, I. Irmansyah, L. Jancoriene,

569   J. Kirwan, S. Kumar, P. Lennon, G. Lopardo, P. Lydon, N. Magrini, T. Maguire, S.

570   Manevska, O. Manuel, S. McGinty, M. T. Medina, M. L. Mesa Rubio, M. C. Miranda-

571   Montoya, J. Nel, E. P. Nunes, M. Perola, A. Portoles, M. R. Rasmin, A. Raza, H. Rees, P.

572   P. S. Reges, C. A. Rogers, K. Salami, M. I. Salvadori, N. Sinani, J. A. C. Sterne, M.

573   Stevanovikj, E. Tacconelli, K. A. O. Tikkinen, S. Trelle, H. Zaid, J. A. Rottingen, S.

574   Swaminathan, Repurposed Antiviral Drugs for Covid-19 - Interim WHO Solidarity Trial

575   Results. *N Engl J Med*, (2020).

576 28. A. Pizzorno, B. Padey, J. Dubois, T. Julien, A. Traversier, V. Duliere, P. Brun, B. Lina, M.

577   Rosa-Calatrava, O. Terrier, In vitro evaluation of antiviral activity of single and combined

578   repurposable drugs against SARS-CoV-2. *Antiviral Res* **181**, 104878 (2020).

579 29. D. E. Gordon, G. M. Jang, M. Bouhaddou, J. Xu, K. Obernier, K. M. White, M. J. O'Meara,

580   V. V. Rezelj, J. Z. Guo, D. L. Swaney, T. A. Tummino, R. Huttenhain, R. M. Kaake, A. L.

581   Richards, B. Tutuncuoglu, H. Foussard, J. Batra, K. Haas, M. Modak, M. Kim, P. Haas, B.

582   J. Polacco, H. Braberg, J. M. Fabius, M. Eckhardt, M. Soucheray, M. J. Bennett, M. Cakir,

583   M. J. McGregor, Q. Li, B. Meyer, F. Roesch, T. Vallet, A. Mac Kain, L. Miorin, E. Moreno,

584   Z. Z. C. Naing, Y. Zhou, S. Peng, Y. Shi, Z. Zhang, W. Shen, I. T. Kirby, J. E. Melnyk, J.

585   S. Chorba, K. Lou, S. A. Dai, I. Barrio-Hernandez, D. Memon, C. Hernandez-Armenta, J.

586   Lyu, C. J. P. Mathy, T. Perica, K. B. Pilla, S. J. Ganesan, D. J. Saltzberg, R. Rakesh, X.

587   Liu, S. B. Rosenthal, L. Calviello, S. Venkataramanan, J. Liboy-Lugo, Y. Lin, X. P. Huang,

588   Y. Liu, S. A. Wankowicz, M. Bohn, M. Safari, F. S. Ugur, C. Koh, N. S. Savar, Q. D. Tran,

589   D. Shengjuler, S. J. Fletcher, M. C. O'Neal, Y. Cai, J. C. J. Chang, D. J. Broadhurst, S.

590   Klippsten, P. P. Sharp, N. A. Wenzell, D. Kuzuoglu-Ozturk, H. Y. Wang, R. Trenker, J.

591   M. Young, D. A. Cavero, J. Hiatt, T. L. Roth, U. Rathore, A. Subramanian, J. Noack, M.

592   Hubert, R. M. Stroud, A. D. Frankel, O. S. Rosenberg, K. A. Verba, D. A. Agard, M. Ott,

593   M. Emerman, N. Jura, M. von Zastrow, E. Verdin, A. Ashworth, O. Schwartz, C. d'Enfert,

594   S. Mukherjee, M. Jacobson, H. S. Malik, D. G. Fujimori, T. Ideker, C. S. Craik, S. N. Floor,

595   J. S. Fraser, J. D. Gross, A. Sali, B. L. Roth, D. Ruggero, J. Taunton, T. Kortemme, P.

596   Beltrao, M. Vignuzzi, A. Garcia-Sastre, K. M. Shokat, B. K. Shoichet, N. J. Krogan, A

597   SARS-CoV-2 protein interaction map reveals targets for drug repurposing. *Nature* **583**,

598   459-468 (2020).

599   30.   R. Tian, A. J. Samelson, V. V. Rezelj, M. Chen, G. N. Ramadoss, X. Guo, A. M. Kain, Q.

600   D. Tran, S. A. Lim, I. Lui, J. Nunez, S. J. Rockwood, N. Liu, J. Carlson-Stevermer, J. Oki,

601   T. Maures, K. Holden, J. S. Weissman, J. A. Wells, B. Conklin, M. Vignuzzi, M.

602   Kampmann, BRD2 inhibition blocks SARS-CoV-2 infection in vitro by reducing

603   transcription of the host cell receptor ACE2. *bioRxiv*, (2021).

604   31.   T. C. Chou, Theoretical basis, experimental design, and computerized simulation of

605   synergism and antagonism in drug combination studies. *Pharmacol Rev* **58**, 621-681

606   (2006).

607   32.   T. C. Chou, Derivation and properties of Michaelis-Menten type and Hill type equations

608   for reference ligands. *J Theor Biol* **59**, 253-276 (1976).

609   33.   T. C. Chou, P. Talalay, Quantitative analysis of dose-effect relationships: the combined

610   effects of multiple drugs or enzyme inhibitors. *Adv Enzyme Regul* **22**, 27-55 (1984).

611   34.   R. T. Eastman, J. S. Roth, K. R. Brimacombe, A. Simeonov, M. Shen, S. Patnaik, M. D.

612   Hall, Remdesivir: A Review of Its Discovery and Development Leading to Emergency Use

613   Authorization for Treatment of COVID-19. *ACS Cent Sci* **6**, 672-683 (2020).

614   35.   F. H. Andrews, A. R. Singh, S. Joshi, C. A. Smith, G. A. Morales, J. R. Garlich, D. L.

615   Durden, T. G. Kutateladze, Dual-activity PI3K-BRD4 inhibitor for the orthogonal

616   inhibition of MYC to block tumor growth and metastasis. *Proc Natl Acad Sci U S A* **114**,

617   E1072-E1080 (2017).

618   36.   L. Carlino, G. Rastelli, Dual Kinase-Bromodomain Inhibitors in Anticancer Drug

619   Discovery: A Structural and Pharmacological Perspective. *J Med Chem* **59**, 9305-9320

620   (2016).

621   37.   S. Joshi, A. R. Singh, K. X. Liu, T. V. Pham, M. Zulcic, D. Skola, H. B. Chun, C. K. Glass,

622   G. A. Morales, J. R. Garlich, D. L. Durden, SF2523: Dual PI3K/BRD4 Inhibitor Blocks

623   Tumor Immunosuppression and Promotes Adaptive Immune Responses in Cancer. *Mol*

624   *Cancer Ther* **18**, 1036-1044 (2019).

625   38.   H. Zhu, J. H. Mao, Y. Wang, D. H. Gu, X. D. Pan, Y. Shan, B. Zheng, Dual inhibition of

626   BRD4 and PI3K-AKT by SF2523 suppresses human renal cell carcinoma cell growth.

627   *Oncotarget* **8**, 98471-98481 (2017).

628   39.   G. A. Morales, J. R. Garlich, J. Su, X. Peng, J. Newblom, K. Weber, D. L. Durden,

629   Synthesis and cancer stem cell-based activity of substituted 5-morpholino-7H-thieno[3,2-

630   b]pyran-7-ones designed as next generation PI3K inhibitors. *J Med Chem* **56**, 1922-1939

631   (2013).

632   40.   O. Trott, A. J. Olson, AutoDock Vina: improving the speed and accuracy of docking with

633   a new scoring function, efficient optimization, and multithreading. *J Comput Chem* **31**,

634   455-461 (2010).

635   41.   S. Ruiz-Carmona, D. Alvarez-Garcia, N. Foloppe, A. B. Garmendia-Doval, S. Juhos, P.

636   Schmidtke, X. Barril, R. E. Hubbard, S. D. Morley, rDock: a fast, versatile and open source

637   program for docking ligands to proteins and nucleic acids. *PLoS Comput Biol* **10**, e1003571

638   (2014).

639 42. Q. Zhang, L. Zeng, C. Shen, Y. Ju, T. Konuma, C. Zhao, C. R. Vakoc, M. M. Zhou,
640   Structural Mechanism of Transcriptional Regulator NSD3 Recognition by the ET Domain
641   of BRD4. *Structure* **24**, 1201-1208 (2016).

642 43. J. F. Chan, Y. Yao, M. L. Yeung, W. Deng, L. Bao, L. Jia, F. Li, C. Xiao, H. Gao, P. Yu,
643   J. P. Cai, H. Chu, J. Zhou, H. Chen, C. Qin, K. Y. Yuen, Treatment With
644   Lopinavir/Ritonavir or Interferon-beta1b Improves Outcome of MERS-CoV Infection in a
645   Nonhuman Primate Model of Common Marmoset. *J Infect Dis* **212**, 1904-1913 (2015).

646 44. V. C. Cheng, B. S. Tang, A. K. Wu, C. M. Chu, K. Y. Yuen, Medical treatment of viral
647   pneumonia including SARS in immunocompetent adult. *J Infect* **49**, 262-273 (2004).

648 45. K. K. To, O. T. Tsang, W. S. Leung, A. R. Tam, T. C. Wu, D. C. Lung, C. C. Yip, J. P.
649   Cai, J. M. Chan, T. S. Chik, D. P. Lau, C. Y. Choi, L. L. Chen, W. M. Chan, K. H. Chan,
650   J. D. Ip, A. C. Ng, R. W. Poon, C. T. Luo, V. C. Cheng, J. F. Chan, I. F. Hung, Z. Chen,
651   H. Chen, K. Y. Yuen, Temporal profiles of viral load in posterior oropharyngeal saliva
652   samples and serum antibody responses during infection by SARS-CoV-2: an observational
653   cohort study. *Lancet Infect Dis* **20**, 565-574 (2020).

654 46. J. Dunning, J. K. Baillie, B. Cao, F. G. Hayden, R. International Severe Acute, C. Emerging
655   Infection, Antiviral combinations for severe influenza. *Lancet Infect Dis* **14**, 1259-1270
656   (2014).

657 47. I. F. N. Hung, K. K. W. To, J. F. W. Chan, V. C. C. Cheng, K. S. H. Liu, A. Tam, T. C.
658   Chan, A. J. Zhang, P. Li, T. L. Wong, R. Zhang, M. K. S. Cheung, W. Leung, J. Y. N. Lau,
659   M. Fok, H. Chen, K. H. Chan, K. Y. Yuen, Efficacy of Clarithromycin-Naproxen-
660   Oseltamivir Combination in the Treatment of Patients Hospitalized for Influenza A(H3N2)

661   Infection: An Open-label Randomized, Controlled, Phase IIb/III Trial. *Chest* **151**, 1069-

662   1080 (2017).

663 48. C. R. Rayner, L. Dron, J. J. H. Park, E. H. Decloedt, M. F. Cotton, V. Niranjan, P. F. Smith,

664   M. G. Dodds, F. Brown, G. Reis, D. Wesche, E. J. Mills, Accelerating Clinical Evaluation

665   of Repurposed Combination Therapies for COVID-19. *Am J Trop Med Hyg* **103**, 1364-

666   1366 (2020).

667 49. I. F. Hung, K. C. Lung, E. Y. Tso, R. Liu, T. W. Chung, M. Y. Chu, Y. Y. Ng, J. Lo, J.

668   Chan, A. R. Tam, H. P. Shum, V. Chan, A. K. Wu, K. M. Sin, W. S. Leung, W. L. Law,

669   D. C. Lung, S. Sin, P. Yeung, C. C. Yip, R. R. Zhang, A. Y. Fung, E. Y. Yan, K. H. Leung,

670   J. D. Ip, A. W. Chu, W. M. Chan, A. C. Ng, R. Lee, K. Fung, A. Yeung, T. C. Wu, J. W.

671   Chan, W. W. Yan, W. M. Chan, J. F. Chan, A. K. Lie, O. T. Tsang, V. C. Cheng, T. L.

672   Que, C. S. Lau, K. H. Chan, K. K. To, K. Y. Yuen, Triple combination of interferon beta-

673   1b, lopinavir-ritonavir, and ribavirin in the treatment of patients admitted to hospital with

674   COVID-19: an open-label, randomised, phase 2 trial. *Lancet* **395**, 1695-1704 (2020).

675 50. P. K. Panda, A. Bandyopadhyay, B. C. Singh, B. Moirangthem, G. Chikara, S. Saha, Y. A.

676   Bahurupi, Safety and efficacy of antiviral combination therapy in symptomatic patients of

677   Covid-19 infection - a randomised controlled trial (SEV-COVID Trial): A structured

678   summary of a study protocol for a randomized controlled trial. *Trials* **21**, 866 (2020).

679 51. Q. Fan, B. Zhang, J. Ma, S. Zhang, Safety profile of the antiviral drug remdesivir: An

680   update. *Biomed Pharmacother* **130**, 110532 (2020).

681 52. Q. Niu, Z. Liu, E. Alamer, X. Fan, H. Chen, J. Endsley, B. B. Gelman, B. Tian, J. H. Kim,

682   N. L. Michael, M. L. Robb, J. Ananworanich, J. Zhou, H. Hu, Structure-guided drug design

683   identifies a BRD4-selective small molecule that suppresses HIV. *J Clin Invest* **129**, 3361-
684   3373 (2019).

685 53. V. S. Mandala, M. J. McKay, A. A. Shcherbakov, A. J. Dregni, A. Kolocouris, M. Hong,
686   Structure and drug binding of the SARS-CoV-2 envelope protein transmembrane domain
687   in lipid bilayers. *Nat Struct Mol Biol* **27**, 1202-1208 (2020).

688 54. M. S. Rahman, M. N. Hoque, M. R. Islam, I. Islam, I. D. Mishu, M. M. Rahaman, M.
689   Sultana, M. A. Hossain, Mutational insights into the envelope protein of SARS-CoV-2.
690   *Gene Rep* **22**, 100997 (2021).

691 55. N. Wang, R. Wu, D. Tang, R. Kang, The BET family in immunity and disease. *Signal*
692   *Transduct Target Ther* **6**, 23 (2021).

693 56. A. Husain, S. N. Byrareddy, Rapamycin as a potential repurpose drug candidate for the
694   treatment of COVID-19. *Chem Biol Interact* **331**, 109282 (2020).

695 57. J. Dyall, R. Gross, J. Kindrachuk, R. F. Johnson, G. G. Olinger, Jr., L. E. Hensley, M. B.
696   Frieman, P. B. Jahrling, Middle East Respiratory Syndrome and Severe Acute Respiratory
697   Syndrome: Current Therapeutic Options and Potential Targets for Novel Therapies. *Drugs*
698   **77**, 1935-1966 (2017).

699 58. G. R. Campbell, R. S. Bruckman, S. D. Herns, S. Joshi, D. L. Durden, S. A. Spector,
700   Induction of autophagy by PI3K/MTOR and PI3K/MTOR/BRD4 inhibitors suppresses
701   HIV-1 replication. *J Biol Chem* **293**, 5808-5820 (2018).

702 59. H. M. Berman, J. Westbrook, Z. Feng, G. Gilliland, T. N. Bhat, H. Weissig, I. N.
703   Shindyalov, P. E. Bourne, The Protein Data Bank. *Nucleic Acids Res* **28**, 235-242 (2000).

704   60.   E. J. Mendoza, K. Manguiat, H. Wood, M. Drebot, Two Detailed Plaque Assay Protocols

705   for the Quantification of Infectious SARS-CoV-2. *Curr Protoc Microbiol* **57**, ecpmc105

706   (2020).

707   61.   T. C. Chou, Drug combination studies and their synergy quantification using the Chou-

708   Talalay method. *Cancer Res* **70**, 440-446 (2010).

709   62.   A. Ianevski, A. K. Giri, T. Aittokallio, SynergyFinder 2.0: visual analytics of multi-drug

710   combination synergies. *Nucleic Acids Res* **48**, W488-W493 (2020).

723   **Author contributions:**

724   Conceptualization: DLD, SNB.

725   Methodology: AA, SNB, TGK, SNB.

726   Investigation: AA, KP, MT, KRV

727   Data analysis: AA, KP, MT, KRV, KBC, TGK, DLD, SNB

728   Funding acquisition: SNB

729   Writing – original draft: AA, SNB, DLD, TGK, GAM

730   Writing – review & editing: AA, KP, MT, KBC, KRV, TGK, DLD, SNB, GAM.

731   **Competing interests:** DLD and GMA declare financial interest in SF2523 via their holding in

732   SignalRx Pharmaceuticals, Inc.

733   **Data and materials availability:** All data related with this study are presented in the manuscript

734   or the supplementary materials.

735

736

737

738

739

740

741

742

743

744

745

746

747

748

749

750

751 **Figures**

752
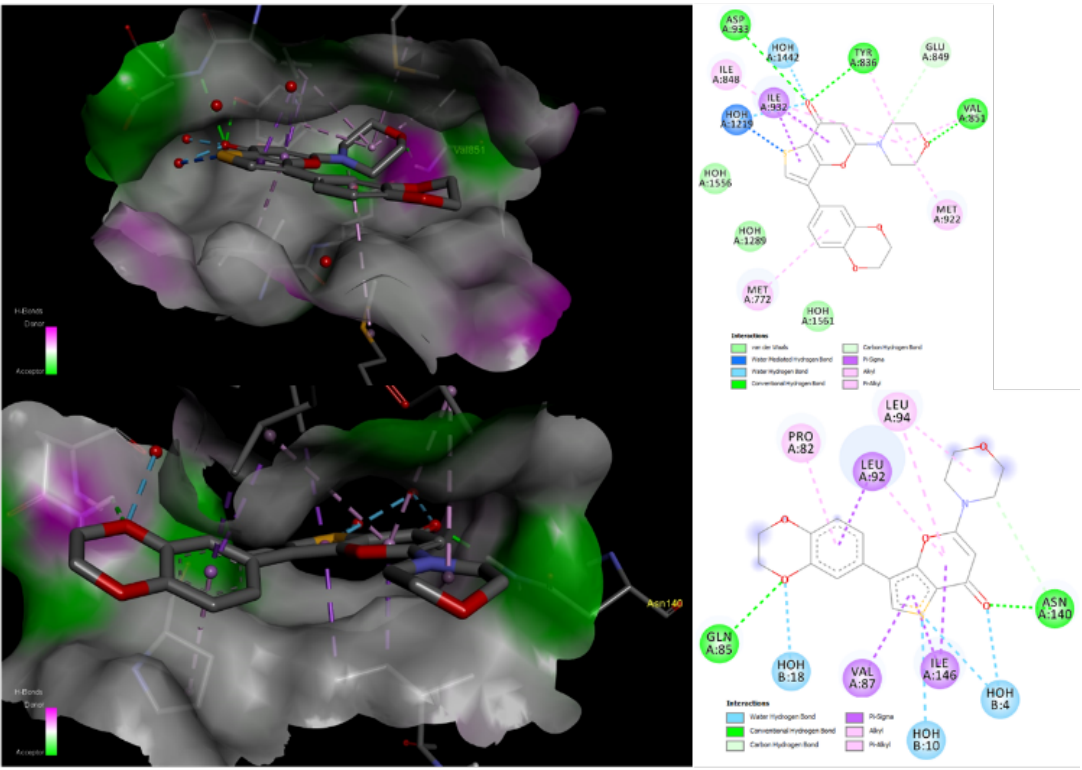
BRD2-1*	BRD2-2*	BRD4-1	BRD4-2	PI3Kα	PI3Kβ	PI3Kδ	PI3Kγ	mTor
190	800	79	732	13	214	12	158	280

753   * = Kd (nM)

754   **Fig. 1.** Predicted binding (docking) of SF2523 in PI3K-α catalytic domain (upper panel) and

755   observed binding in crystal structure of SF2523 bound to BRD4-BD1 acetyl lysine binding site

756   (1.8 Angstroms resolution) (bottom panel). *In vitro* (enzymatic) potency of SF2523 against

757   targets.

758

759

760   **Fig 2. SARS-CoV-2 viral loads and dose-response curve in SF2523 and remdesivir treated**

761   **and SARS-CoV-2 infected UNCN1T cells and Vero-STAT1 knockout cells.** (A & B) Real-

762   time quantitative PCR analysis of SARS-CoV-2 genome equivalent per ml of culture supernatant

763   after 24 hrs post-infection in SF2523 (in blue) and remdesivir (in green) treated UNCN1T cells

764   and Vero-STAT1 knockout cells with indicated drug concentrations, respectively. (C & D)

765   SF2523 (in blue) and remdesivir (in green) dose response curve by percentage inhibition of

766   SARS-CoV-2 replication 24 hrs post infection in UNCN1T cells and Vero-STAT1 knockout

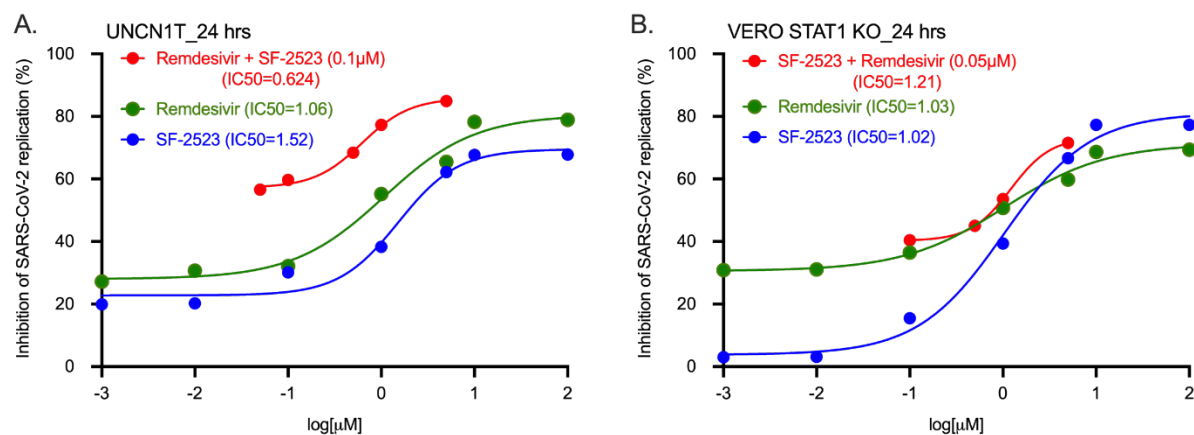767   cells with indicated drug concentrations, respectively.

768

769

770

771   **Fig 3. Dose-response curve for single and combination of SF2523 and remdesivir in SARS-**

772   **CoV-2 infected UNCN1T cells and Vero-STAT1 knockout cells 24 hrs post infection.** (**A**)

773   Dose response curve of remdesivir (green: IC_{50} = 1.06 µM), (blue: IC_{50} = 1.52 µM), and

774   remdesivir with a fixed dose combination of SF2523 (0.1 µM) (red: IC_{50} = 0.625) by percentage

775   inhibition of SARS-CoV-2 replication 24 hrs post infection in UNCN1T cells; (**B**) Dose response

776   curve of remdesivir (green: IC_{50} = 1.03µM), (blue: IC_{50} = 1.02 µM), and SF2523 with a fixed

777   dose combination of remdesivir (0.05µM) (red: IC_{50} = 1.21) by percentage inhibition of SARS-

778   CoV-2 replication 24 hrs post infection (IC_{50} = 1.02 µM) in Vero-STAT1 knockout cells.
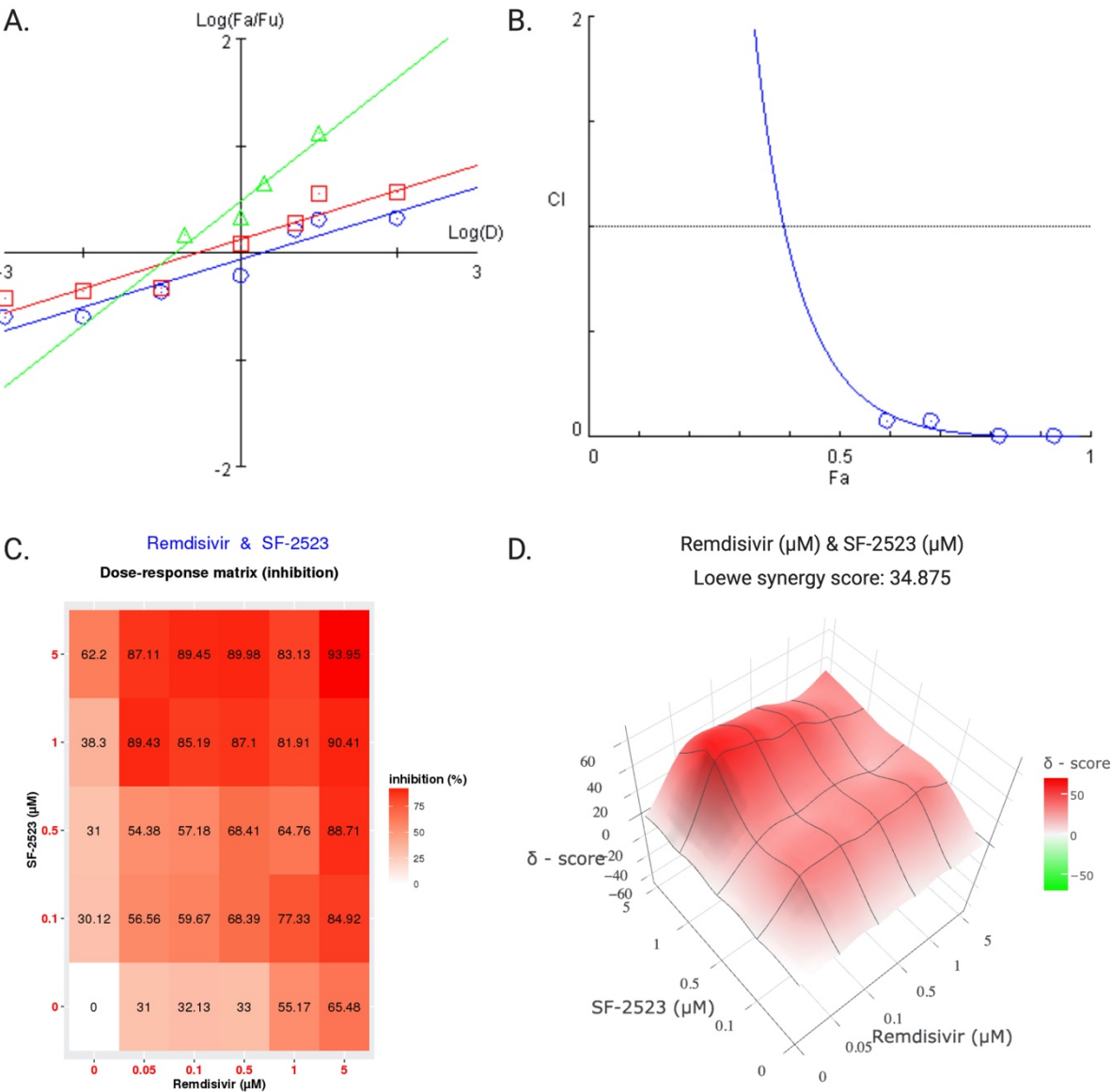
779

780

781

782

783

784

785

786

Fig 4. Synergistic effect of remdesivir and SF2523 combined treatment against SARS-CoV-2 infected UNCN1T cells 24 hrs post infection. (A) The Median-Effect plot (Chou plot) of remdesivir (the red line with square data points, SF2523 (blue line with circular data points) and fixed dose combination of remdesivir and SF2523 (green line with triangular data points). The median-Effect equation, that describes the dose-effect relationship is given by $(Fa/Fu) = (D/Dm)^m$ or $\log(Fa/Fu) = m \log(D) - m \log(Dm)$. The slope (m) of the lines signifies the shape (m = 1, >1, and <1 signify hyperbolic, sigmoidal, and flat sigmoidal dose-effect curves respectively). Fa is defined as percentage inhibition of viral growth at dose D and Fu is the fraction that remain unaffected (i.e., Fu = 1 - Fa). The antilog of x-intercept, where Fa/Fu = 1 or $\log(Fa/Fu) = 0$, gives the Dm value. [log(Dm)] signifies the potency of the drugs (where Dm stands for median effective dose or IC_{50} concentration: The concentration required to inhibit 50% growth of the virus). **(B)** Combination index plot or Chou-Talaly plot or Fa-CI plot: A plot of CI (combination index) on the Y-axis vs Fa on X-axis for fixed dose combination of remdesivir and SF2523 in SARS-CoV-2 infected UNCN1T cells (blue line with circular data points); Low CI values with increase in Fa values indicates superior compatibility and high synergism between drugs combination (based on Chou and Talalay Combination Index Theorem, CI < 1, = 1, and >1 indicate synergism, additive effect, and antagonism, respectively). **(C)** Dose-response percent inhibition matrix of single and combined treatment of remdesivir and SF2523 in SARS-CoV-2 infected UNCN1T cells 24 hrs post infection. **(D)** 3-D interaction landscape between remdesivir and SF2523 calculated based on Loewe additive model using SynergyFinder v.2 in SARS-CoV-2 infected UNCN1T cells 24 hrs post infection (Loewe synergy score 34.88; with most synergistic area score of 40.24). Synergy maps highlight synergistic and antagonistic dose regions in red and green colors, respectively. Although there is no defined threshold, for drug

810   combinations with a synergy scores above -10 is considered likely antagonistic, score between -

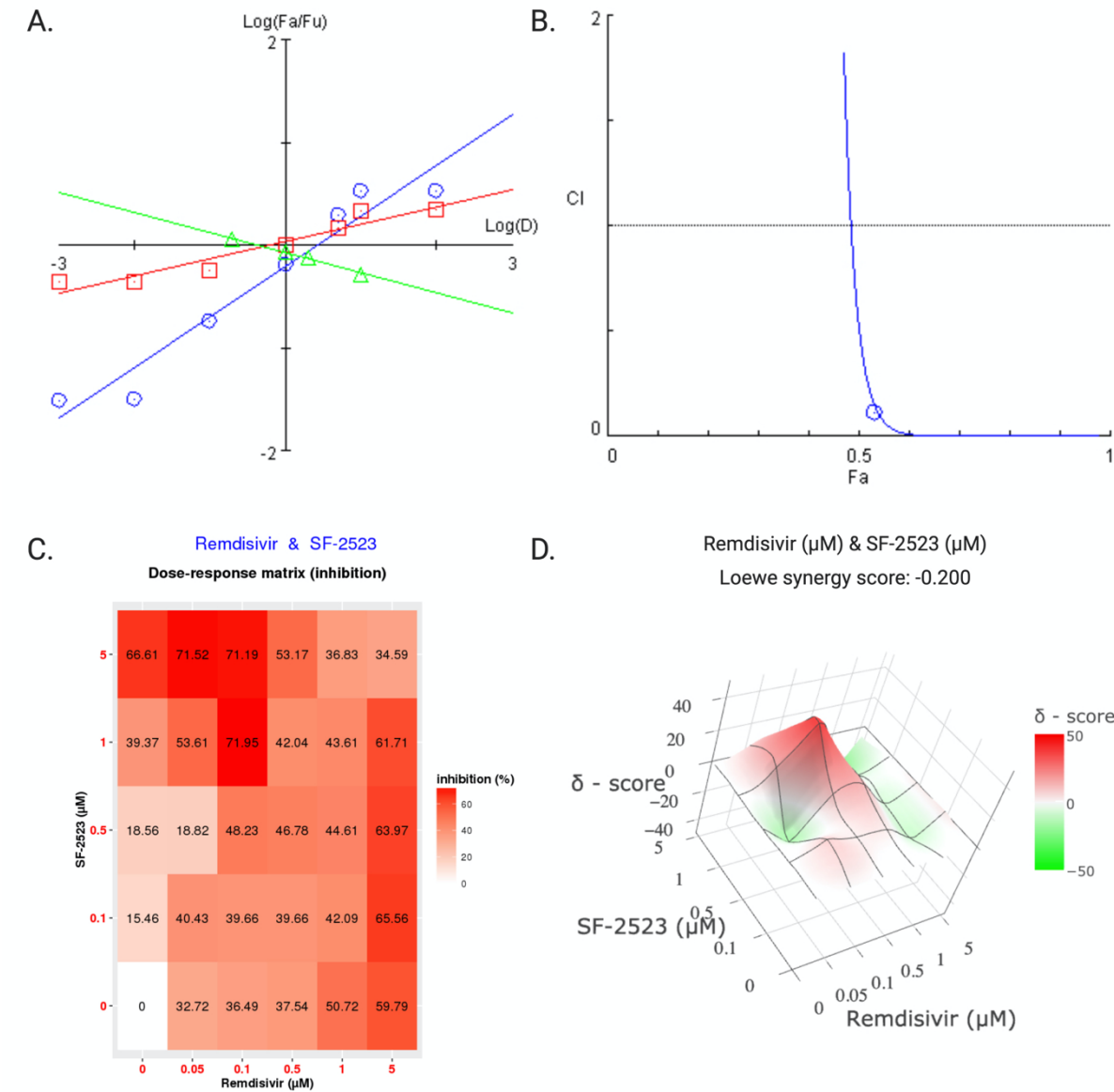811   10 to 10 is considered likely additive and score above 10 is considered synergistic.

812

813

Fig 5. Synergistic effect of remdesivir and SF2523 combined treatment against SARS-CoV-

2 in Vero-STAT1 knockout cells 24 hrs post infection. (A) The Median-Effect plot (Chou

plot) of remdesivir (the red line with square data points, SF2523 (blue line with circular data

817   points) and fixed dose combination of remdesivir and SF2523 (green line with triangular data

818   points). The median-Effect equation, that describes the dose-effect relationship is given by

819    $(Fa/Fu) = (D/Dm)^m$ or $\log(Fa/Fu) = m \log(D) - m \log(Dm)$. The slope (m) of the lines signifies

820   the shape (m = 1, >1, and <1 signify hyperbolic, sigmoidal, and flat sigmoidal dose-effect curves

821   respectively). Fa is defined as percentage inhibition of viral growth at dose D and Fu is the

822   fraction that remain unaffected (i.e., Fu = 1 - Fa). The antilog of x-intercept, where Fa/Fu = 1 or

823    $\log(Fa/Fu) = 0$, gives the Dm value. [log(Dm)] signifies the potency of the drugs (where Dm

824   stands for median effective dose or IC_{50} concentration: The concentration required to inhibit 50%

825   growth of the virus). (**B**) Combination index plot or Chou-Talaly plot or Fa-CI plot: A plot of CI

826   (combination index) on the Y-axis vs Fa on X-axis for fixed dose combination of remdesivir and

827   SF2523 in SARS-CoV-2 infected Vero-STAT1 knockout cells (blue line with circular data

828   points); Low CI values with increase in Fa values indicates superior compatibility and high

829   synergism between drugs combination (based on Chou and Talalay Combination Index Theorem,

830   CI < 1, = 1, and >1 indicate synergism, additive effect, and antagonism, respectively). (**C**) Dose-

831   response percent inhibition matrix of single and combined treatment of remdesivir and SF2523

832   in SARS-CoV-2 infected Vero-STAT1 knockout cells 24 hrs post infection. (**D**) 3-D interaction

833   landscape between remdesivir and SF2523 calculated based on Loewe additive model using

834   SynergyFinder v.2 in SARS-CoV-2 infected Vero-STAT1 knockout cells 24 hrs post infection

835   (Loewe synergy score -0.20; with most synergistic area score of 7.67). Synergy maps highlight

836   synergistic and antagonistic dose regions in red and green colors, respectively. Although there is

837   no defined threshold, for drug combinations with a synergy scores above -10 is considered likely

838   antagonistic, score between -10 to 10 is considered likely additive and score above 10 is
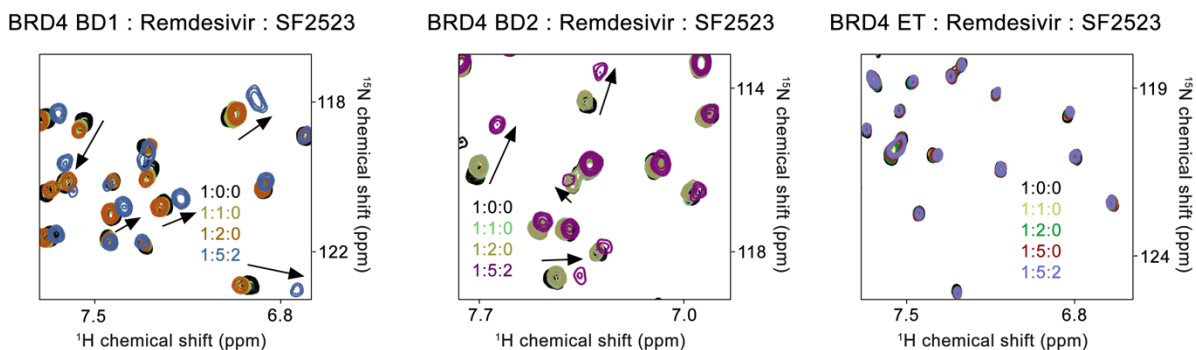
839   considered synergistic.

Fig 6. Remdesivir does not bind to the BRD4 BD domains and does not affect binding of SF2523 to BDs. Superimposed ^{1}H,^{15}N HSQC spectra of uniformly ^{15}N-labeled BD1 (left), BD2 (middle) and ET (right) domains of BRD4 with the indicated ligands added in a stepwise manner. The spectra are color coded according to the protein:ligand ratios. Small resonance changes are due to weak binding of DMSO, which was confirmed by titrating DMSO alone to separate samples of these domains (data not shown).
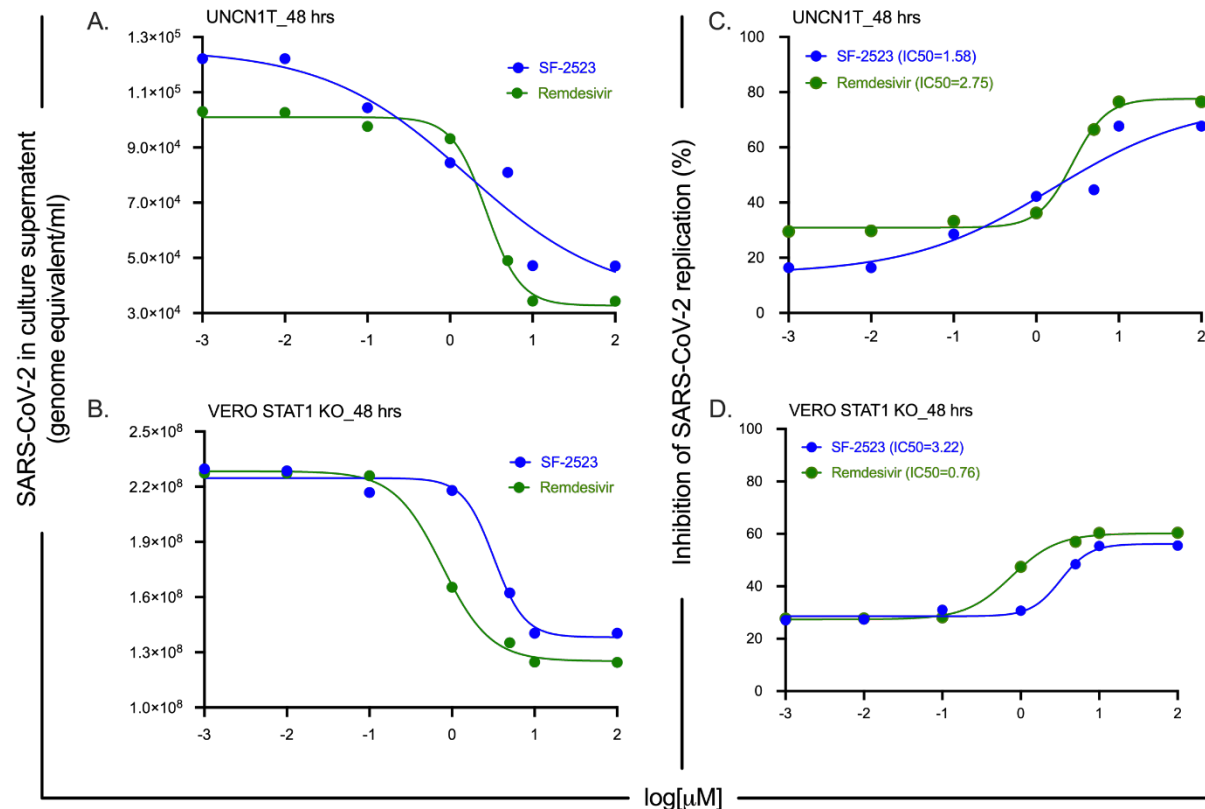
Fig S1. SARS-CoV-2 viral loads and dose-response curve in SF2523 and remdesivir treated and SARS-CoV-2 infected UNCN1T cells and Vero-STAT1 knockout cells. (**A & B**) Real-time quantitative PCR analysis of SARS-CoV-2 genome equivalent per ml of culture supernatant after 48 hrs post-infection in SF2523 (in blue) and remdesivir (in green) treated UNCN1T cells and Vero-STAT1 knockout cells with indicated drug concentrations respectively. (**C & D**) SF2523 (in blue) and remdesivir (in green) dose response curve by percentage inhibition of SARS-CoV-2 replication 48 hrs post infection in UNCN1T cells and Vero-STAT1 knockout cells with indicated drug concentrations respectively. In UNCN1T cells, SF2523 has an IC_{50} of 1.58 μM and remdesivir has an IC_{50} of 2.75 μM; In Vero-STAT1 knockout cells, SF2523 has an IC_{50} of 3.22 μM and remdesivir has an IC_{50} of 0.76 μM.

863 **Table 1: The median effective dose of individual compounds and their combination**

Vero-STAT1 knockout Cells			
Drug/Combo	**Dm**	**m**	**r**
SF2523 (S)	2.617	0.492	0.971
Remdesivir (R)	0.533	0.167	0.955
Combination (SRF)	0.452	-0.197	-0.994

UNCN1T Cells			
Drug/Combo	**Dm**	**m**	**r**
SF2523 (S)	1.836	0.222	0.953
Remdesivir (R)	0.272	0.231	0.949
Combination (SRF)	0.145	0.577	0.967

864 Dm: The median effective dose; m: The slope of the median effect (ME) plot; r: The linear correlation

865 coefficient of ME plot.

866

867 **Table 2: The CI values at different simulated effective dose of fixed dose combination of**

868 **SF2523 and remdesivir**

	CI values			
	ED50	ED75	ED90	ED95
Vero-STAT1 knockout cells	0.5105	3.75E-05	1.44E-08	7.10E-11
UNCN1T cells	0.3054	0.0173	9.91E-04	1.42E-04

869

43